Characterization of iron oxides by x-ray absorption at the oxygen *K* edge using a full multiple-scattering approach

Z. Y. Wu
Institut des Matériaux de Nantes, CNRS UMR 110, Laboratoire de Chimie des Solides, 2 rue de la Houssinière, 44072 Nantes Cedex 03, France
and Istituto Nazionale di Fisica Nucleare, Laboratori Nazionali di Frascati, P.O. Box 13, 00044 Frascati, Italy

S. Gota, F. Jollet, M. Pollak, and M. Gautier-Soyer
Commissariat à l'Energie Atomique, DSM/DRECAM/SRSIM, Batiment 462, CE Saclay, 91191 Gif-sur Yvette Cedex, France

C. R. Natoli
Istituto Nazionale di Fisica Nucleare, Laboratori Nazionali di Frascati, P.O. Box 13, 00044 Frascati, Italy
(Received 14 May 1996)

α-Fe_2O_3, Fe_3O_4, and FeO compounds are characterized by means of x-ray-absorption near-edge-structure spectroscopy at the oxygen *K* edge. Using increasing cluster sizes around the excited atom in the full multiple-scattering simulations, we are able to link the features present in the spectra of each iron oxide to its specific atomic arrangement and electronic structure. The prepeak structure is successfully reproduced and interpreted as transitions from the oxygen $1s$ core state to antibonding oxygen $2p$ states hybridized with Fe $3d$ orbitals. Their intensity and shape depends on the Fe site symmetry, the occupation number of the *d* levels, and the O-Fe bond length of each different iron oxide. Higher lying spectral features are shown to be related to scattering of the photoelectron by a particular oxygen shell and an extended x-ray absorption fine structure–like relation is established between their energy position and the distance of the corresponding shell from the photoabsorber. [S0163-1829(97)00403-7]

I. INTRODUCTION

Iron oxides are important technological materials, utilized in areas such as heterogeneous catalysis and high-density recording media. Nevertheless, a lot remains to be learned about their fundamental properties because of their complexity, which mainly derives from the number of stable iron oxides with different atomic structure, electronic configuration, and ranges of thermodynamic stability.[1] They are all interconvertible at different temperatures and oxygen pressures. Of the common forms, α-Fe_2O_3 (hematite) has the rhombohedral crystal structure of corundum with Fe^{3+} cations located in distorted oxygen octahedra of the rhombohedral lattice. Fe_3O_4 (magnetite) has the cubic inverse spinel structure with Fe^{2+} cations in octahedral sites and Fe^{3+} cations in both octahedral and tetrahedral sites, surrounded by oxygen ions. FeO (wüstite) crystallizes in the NaCl structure with a tendency to be defective in iron, and contains Fe^{2+} cations octahedrally coordinated to the oxygen anions. In the present paper, we present a systematic study on α-Fe_2O_3, Fe_3O_4, and FeO by means of x-ray absorption spectroscopy (XAS). X-ray absorption is a local process in which a core level electron is promoted to an excited electronic state, which can be coupled to the original core level by the dipole selection rule. For the oxygen *K* edge ($l = 0$), this means that only oxygen *p* character states ($l = 1$) can be reached. X-ray absorption near edge structure (XANES) spectra are commonly interpreted in terms of two complementary ways, namely, the empty state electronic structure approach and the multiple scattering one.

O *K*-edge spectra of iron oxides have already been recorded either by means of electron energy loss near edge structure spectroscopy[2–4] or by XANES spectroscopy.[5–7] The shape of the spectra has been shown to be particularly sensitive to the nature of the $3d$ transition metal (TM) oxides.[7,8] Colliex *et al.*[2] have compared the O *K*-edge fine structure of α-Fe_2O_3, Fe_3O_4, and FeO over a wide energy range extending up to 40–50 eV above the threshold. Unfortunately, their energy resolution (1 eV) does not allow us to reach all the details of the spectra, especially the prepeak structure. Paterson and Krivanek[3] have recorded with improved resolution (0.3–0.4 eV) the fine structure of α- and γ-Fe_2O_3, pointing out that an enhanced resolution provides valuable additional information. Nevertheless they have only measured over the first 20 eV above threshold. The O *K*-edge absorption spectra of α-Fe_2O_3 and Fe_3O_4 from Refs. 2 and 7 present quite similar features and were recorded, respectively, in a total yield and fluorescence detection mode over an energy range of 20 eV above threshold. Nakai *et al.*[6] have measured in similar experimental conditions the O *K*-edge spectra of FeO.

Very recently, some of us have published a detailed comparison of the oxygen *K*-edge absorption spectra of α-Fe_2O_3, Fe_3O_4, and FeO over 50 eV using an energy resolution of 0.5 eV.[9] Starting from this work, we present in this paper the interpretation of the characteristic features of the O *K*-edge spectra in the light of full MS calculations using increasing cluster sizes around the excited oxygen atom. We have connected the specific atomic arrangement and the electronic structure of each iron oxide with the position, shape,

and intensity of the different characteristic features of the spectra. The aim of this work is to set up references for the interpretation of XANES spectra in more complex cases such as modifications of the first atomic planes at the surface (by heat treatments in UHV or under PO_2 pressure, for instance)[9] and ultrathin iron oxide films grown onto a substrate,[10] as it has been done recently at the Fe $L_{2,3}$ edges.[11]

The paper is organized as follows: experimental and calculational details are presented in Secs. II and III, respectively, while Sec. IV is devoted to the presentation of the experimental results. In Sec. V, the results of the calculations for α-Fe_2O_3, Fe_3O_4, and FeO are first discussed, and general tendencies are discussed at the end of the paper.

II. EXPERIMENT

Our α-Fe_2O_3 single crystal was synthesized by Remeika (AT&T Bell Laboratories) using the flux method (Bi_2O_3, B_2O_3). It exhibits a natural growth face having a (1012) orientation, as checked by Laue x-ray diffraction. Fe_3O_4 and FeO single crystals, grown by the zone fusion method, were provided by the Laboratoire de Chimie des Solides (Orsay, France). Samples of Fe_3O_4 were cut along a (111) plane and FeO along (100), and polished. Prior to their loading in the preparation chamber, they were cleaned ultrasonically in ethanol. X-ray absorption experiments were carried out on the SA72 beam line of Super ACO storage ring at the LURE synchrotron facilities (Orsay, France). A toroidal grating monochromator produces an incident photon beam with energies ranging from 150 eV to 900 eV. The total electron yield I was measured by a channeltron placed in front of the irradiated sample. The primary photon beam intensity I_0 was monitored by a second channeltron, which measures the total electron current from a gold grid located in front of the analysis chamber in the path of the photon beam. The I/I_0 ratio was measured as a function of photon energy, ranging from 520 to 580 eV, with a resolution of 0.5 eV.

The spectra of the ''as-received'' samples obtained from total yield detection can confidently be considered as the reference spectra for the said materials, since the x-ray absorption spectroscopy sampling depth, which we estimate to be $\sim$100–200 Å,[12] is large enough to eliminate any significant contribution from the outermost layers, including contaminants. However, as no *in situ* cleaning or checking of the samples was performed, the presence of other oxidation states at the surface cannot be excluded.

III. CALCULATIONAL DETAILS

Our calculations were carried out based on the one-electron full multiple-scattering (MS) theory[13–16] using the CONTINUUM code.[17] We have used the Mattheiss prescription[18] to construct the cluster electronic density and the Coulomb part of the potential by superposition of neutral atomic charge densities obtained either from the Clementi-Roetti tables[19] or generated by the atomic relativistic Hartree-Fock-Slater code of Desclaux.[20] In order to simulate the charge relaxation around the core hole in the photoabsorber of atomic number Z, we have used the screened $Z+1$ approximation (final state rule),[21] which consists in taking the orbitals of the $Z+1$ atom and in constructing the final state charge density by using the excited configuration of the photoabsorber with the core electron promoted to a valence orbital.

For the exchange-correlation part of the potential, we have used the energy- and position-dependent complex Hedin-Lundquist (H-L) self-energy $\Sigma(\vec{r},E)$ as illustrated by Tyson *et al.*[22] The imaginary part of the H-L potential gives the amplitude attenuation of the excited photoelectronic wave due to extrinsic inelastic losses, and takes automatically into account the photoelectron mean free path in the excited final state. The calculated spectra are further convoluted with a Lorentzian function with a full width Γ_h to account for the core hole lifetime.[23] For the sake of the arguments presented here, similar results are obtained by performing the calculation using a $X\alpha$ type of exchange followed by a Lorentzian convolution to account for inelastic losses of the photoelectron in the final state and the core hole width. In this latter case, the total width of the Lorentzian is given by $\Gamma_{\rm tot}(E)=2{\rm Im}\Sigma(E)+\Gamma_h$ where $\Sigma(E)$ is a volume averaged value over the unit cell of the compound of $\Sigma(\vec{r},E)$ as suggested by Penn.[24] We have chosen the muffin-tin radii according to the criterion of Norman,[25] allowing a 10% overlap between contiguous spheres to simulate the atomic bond.

IV. RESULTS

Oxygen K-edge spectra of the ''as-received'' samples of α-Fe_2O_3, Fe_3O_4, and FeO are shown in Fig. 1(a). Similar spectra have been recorded for a large number of other samples, which verify that those of Fig. 1(a) are characteristic of α-Fe_2O_3, Fe_3O_4, and FeO. All these spectra display four main features labeled (A, B, C, and D) and they are in good agreement with other published work.[2–8] Their energy positions are listed in Table I. One can divide the spectra in three regions:

(I) The first region (labeled A) is usually called the ''prepeak'' region. The spectra of the three oxides differ quite markedly in the structure of this first feature. For α-Fe_2O_3, there are two components, A_1 and A_2 of approximately equal intensity, clearly separated by 1.3 eV, whereas for Fe_3O_4, A_2 appears only as a shoulder at 0.7 eV to the high energy side of A_1. In the case of FeO, only a single component is seen. We also observe that the relative intensity of feature A, compared with feature B, increases from FeO to α-Fe_2O_3.

(II) The second region presents a strong feature labeled B. The shape of this peak does not change significantly from one iron oxide to another and its energy position has been taken as the energy reference in Table I.

(III) The third region spreads from about 545 to 575 eV and contains two broad peaks labeled C and D which present different shape, energy position and intensity for the three oxides (see Table I).

Figure 1(b) shows MS theoretical computation of the O K-edge XANES spectra for the three oxides. In the case of α-Fe_2O_3, size convergence was obtained using a cluster of 61 atoms. In the case of Fe_3O_4 and FeO, clusters of 69 and

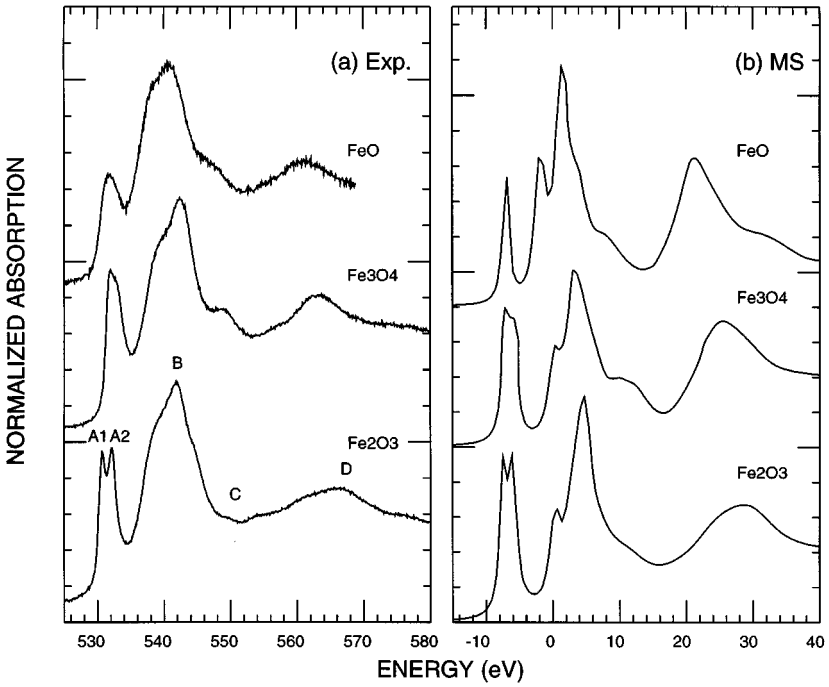

FIG. 1. Experimental (left panel) and MS calculated (right panel) O *K*-edge XANES spectra: α-Fe_2O_3, Fe_3O_4, and FeO.

81 atoms, respectively, were necessary for reaching convergence.

V. DISCUSSION

The comparison of Figs. 1(a) and 1(b) reveals a remarkably good agreement between experimental and calculated O *K*-edge XANES spectra for the three oxides. Nevertheless, the calculations shown in Fig. 1(b) take into account all multiple-scattering paths in a rather big cluster (≈60–80 atoms) and hence do not allow us to assign a particular shell of neighbors to each feature. To elucidate this point, we have to perform MS calculations adding consecutive iron and oxygen shells around the emitter atom. Table II gives the nearest oxygen-iron and oxygen-oxygen distances in Å of α-Fe_2O_3, Fe_3O_4, and FeO compounds, and permits us to easily connect the number of atoms in the cluster with the environment of the oxygen emitter for each MS calculation. In this section, we first discuss our results separately for each oxide.

A. α-Fe_2O_3

In α-Fe_2O_3, oxygen atoms are close packed and Fe^{3+} cations occupy nearly perfect octahedral sites. In Fig. 2, we present theoretical computations of the O *K*-edge XANES spectra in the case of hematite, using different cluster sizes (5, 17, 27, 49, and 61 atoms). For a minimal cluster composed of an O central atom (emitter) surrounded by the four nearest neighbors Fe atoms, the calculated absorption spectrum already shows the presence of the prepeak *A*, although weak. This feature reflects transitions to antibonding O $2p$ states hybridized with the $3d$ metal states, mainly localized at the Fe site.[7] We can observe in the experimental spectra that the feature *A* splits in two components A_1 and A_2. De Groot *et al.*[7] have interpreted these two peaks in a first approximation as the e_g-t_{2g} symmetry bands separated by the ''ligand-field splitting'' (this term denotes the ionic crystal field splitting plus hybridization). Recently, Pollak *et al.*[9] have corroborated this point, by comparison of the oxygen *K* edge spectrum up to 20 eV above the threshold and the O *p* conduction band states obtained from *ab initio* unrestricted Hartree-Fock calculations. This splitting is reproduced by MS calculations when using large clusters as shown in Fig. 2 (27-, 49-, 61-atoms calculations, respectively). In order to illustrate its origin, we present in Fig. 3 a simplified 21-atom cluster calculation, which contains the central oxygen atom, its nearest four Fe atoms, and the outer shell 16 oxygen atoms that provide an octahedral environment for these four

TABLE I. The energy positions in eV of all transition peaks in O *K*-edge XANES spectra of α-Fe_2O_3, Fe_3O_4, and FeO.

	α-Fe_2O_3		Fe_3O_4		FeO	
Peaks	ΔE_{exp} [a]	ΔE_{MS}	ΔE_{exp}	ΔE_{MS}	ΔE_{exp}	ΔE_{MS}
*A*1	−11.1	−12.22	−10.3	−10.21	−9.0	−8.17
*A*2	−9.8	−10.88	−9.6	−9.53		
B	0.0	0.0	0.0	0.0	0.0	0.0
C	7.5	7.48	7.0	7.15	6.8	6.805
D	23.5	23.26	21.5	21.70	20.4	20.44

[a]ΔE is aligned by setting peak *B* to zero on energy scale.

TABLE II. The nearest oxygen-iron and oxygen-oxygen distances in Å of α-Fe_2O_3, Fe_3O_4, and FeO compounds.

	α-Fe_2O_3	Fe_3O_4	FeO
Fe1	1.95 (×2)	1.887 (×1)	2.15 (×6)
Fe2	2.08 (×2)	2.059 (×3)	
O1	2.60 (×2)	2.854 (×3)	3.041 (×12)
O2	2.75 (×2)	2.969 (×6)	
O3	2.88 (×4)	3.082 (×3)	
O4	3.048 (×4)		
⟨O-O⟩	2.868	2.968	3.041

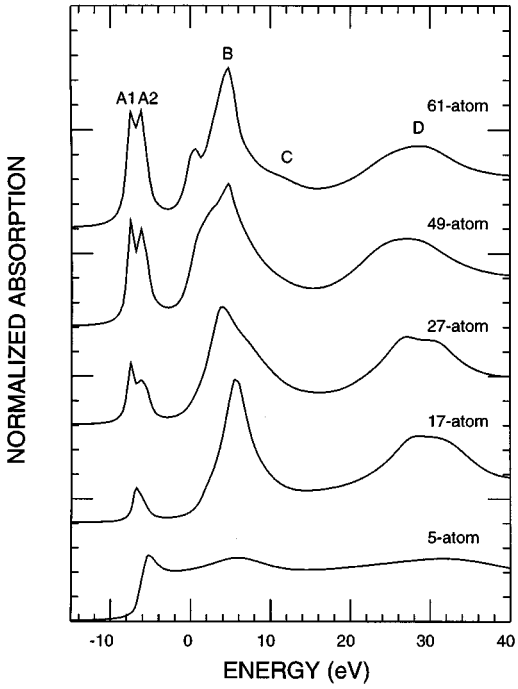

FIG. 2. Theoretical XANES spectra at the O K edge of α-Fe_2O_3 compound as a function of cluster size. The 61-atom cluster includes central oxygen plus 4 Fe, 12 O, 6 Fe, 4 O, 2 Fe, 2 O, 4 Fe, 2 O, 6 Fe, 6 O, 2 Fe, and 10 O atoms (totally 24 iron and 36 oxygen atoms).

Fe. The doublet is very well defined. Therefore, our results also verify that this splitting is due to the local electrostatic interaction of the oxygen charges with the iron d orbitals (crystal field effect). The relative intensities of peaks A_1 and A_2 will be discussed in Sec. V D.

In the language of molecular orbital (MO) theory feature B is generally attributed to oxygen $2p$ states hybridized with iron $4s$ and $4p$ states.[7,26] In the MO level scheme for an octahedral environment these are states of T_{1u} symmetry. The extensive spread in energy for the oxygen $2p$ character

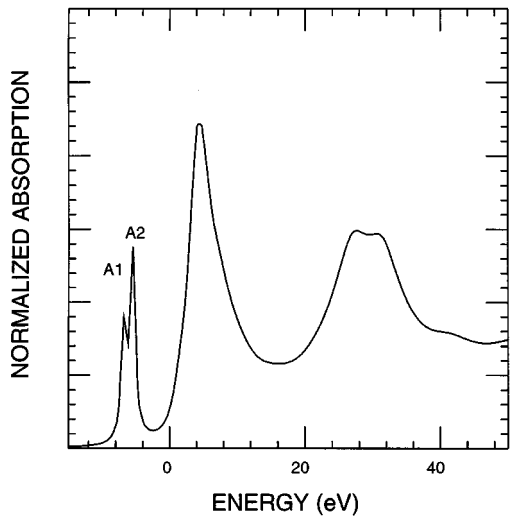

FIG. 3. MS calculation of O K-edge XANES in α-Fe_2O_3 by using a simplified 21-atom cluster: central oxygen plus the nearest four Fe and 16 oxygen atoms.

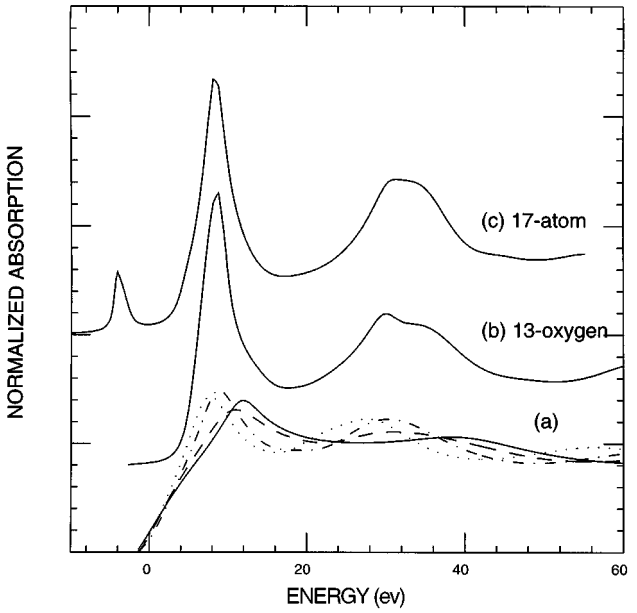

FIG. 4. MS calculations of the oxygen K-edge XANES in α-Fe_2O_3. (a) Simplified calculations from four different nearest oxygen shells: the solid line refers to the scattering contribution from two oxygen atoms located at 2.603 Å from the central excited atom, the dashed line to two oxygen at 2.751 Å, the dash-dot line to four oxygen at 2.885 Å, and the dotted line to four oxygen at 3.048 Å; (b) only a 13 oxygen cluster contribution; (c) 17-atom cluster (13 oxygen plus 4 Fe) MS K-edge spectrum.

is an indication of significant covalence in these oxides. From the point of view of the scattering, the addition of the second shell in our MS calculations (17-atoms cluster), which consists in twelve O atoms distributed among four subshells with slightly different distances (two at 2.60 Å and 2.75 Å and four at 2.88 Å and 3.05 Å), is necessary to reproduce the quite strong peak B as well as the broad peak D. So, these features arise from scattering within the first oxygen atomic shell. This fact demonstrates the relatively strong backscattering of the O^{2-} ions. Figure 4 shows the scattering contribution from each of the four different oxygen neighbor subshells, compared with that from a cluster of only 13 oxygen atoms and from one composed of 17 atoms (13 O atoms plus 4 Fe atoms) calculations. We can see that the peak D is approximately an average of individual scattering contributions while this is not the case for feature B. Therefore we can deduce that the broad appearance of peak D derives from dominantly single-scattering events between absorber and the first oxygen shell of 12 atoms. In contrast, we need to include all MS paths concerning this shell, in order to reproduce the intensity of peak B. Moreover as the only significant changes between the 13 and 17 atoms cluster calculations is the appearance of peak A, this is an additional evidence that the prepeak is associated with the existence of unoccupied O-$2p$ states hybridized with Fe-$3d$ orbitals.

Finally, peak C is reproduced after adding the oxygen shell at about 5.04 Å from the emitter as shown in Fig. 2 by the 61-atom cluster calculation. The additional calculation presented in Fig. 5 by using one single oxygen shell located at 5.04 Å from the absorber proves that feature C comes dominantly from single scattering events between the absorber and this oxygen shell.

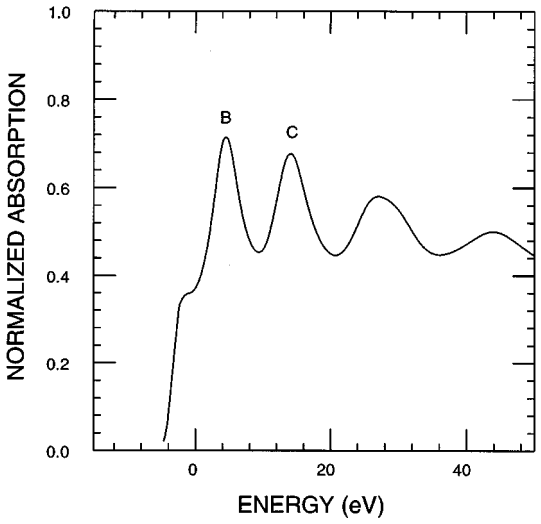

FIG. 5. MS calculation of O *K*-edge XANES in α-Fe_2O_3 by using a simplified atomic cluster: central oxygen plus 10 oxygen atoms located at 5.04 Å.

B. Fe_3O_4

Qualitatively, one might expect a similar explanation for the *A* and *B* peaks in Fe_3O_4 (see Fig. 6). Here the splitting of the *A* component is not well-resolved, and one explanation for this might be that with three Fe sites, two octahedral ones (Fe^{3+} and Fe^{2+}) and the other tetrahedral (Fe^{3+}), each one associated with its e_g-t_{2g}-like splitting, the overall absorption *A* consists of a mixing of several components leading to a loss of resolution. Peak *B* is the dominant contribution and remains rather similar as peak *B* in α-Fe_2O_3. When the oxygen shell located at average 5.141 Å from the central oxygen is included, the feature *C* is very well defined (Fig. 6) at the energy position about 7.15 eV from peak *B*. As can be seen, this peak is quite broader than the one in α-Fe_2O_3, because there are 24 oxygen atoms in this shell, 6 at 5.074 Å and 5.206 Å, and 12 at 5.141 Å, which all give contribution to this peak. Feature *D*, which lies 21.7 eV higher in energy than peak *B*, is associated dominantly with single scattering from the first oxygen shell, as in α-Fe_2O_3.

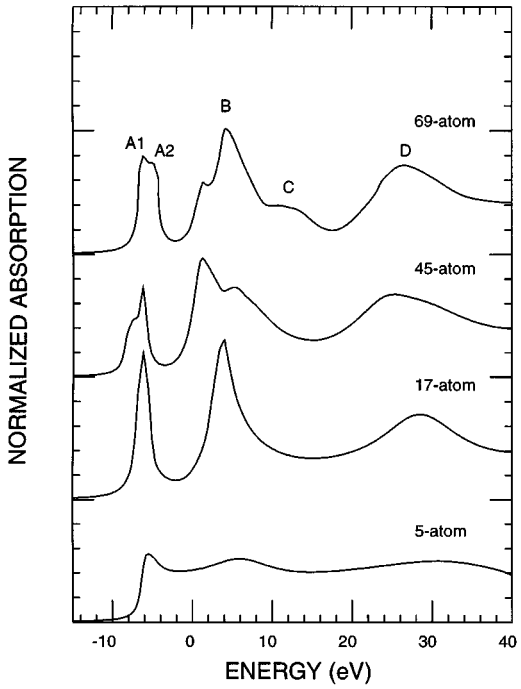

FIG. 6. MS calculations of the oxygen *K*-edge XANES in Fe_3O_4 for different atomic clusters. The 69-atom cluster includes central oxygen plus 4 Fe, 12 O, 7 Fe, 6 O, 15 Fe, and 24 O atoms (totally 26 iron and 42 oxygen atoms).

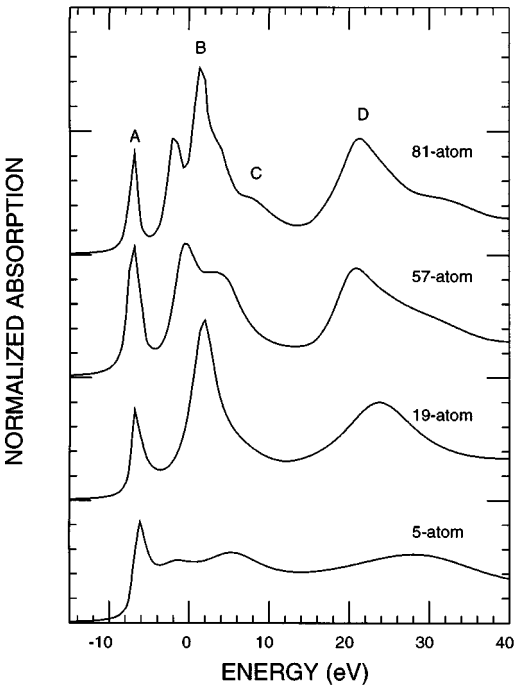

FIG. 7. MS calculations of the O *K*-edge XANES in FeO for different atomic clusters. The 81-atom cluster includes central O plus 6 iron, 12 oxygen, 8 iron, 6 oxygen, 24 iron, and 24 oxygen atoms (totally 38 iron and 42 oxygen atoms).

C. FeO

The results of the calculation for the O *K*-edge XANES spectra of FeO are presented in Fig. 7. Good agreement is obtained with a 81-atom cluster which includes all atoms within 5.266 Å from the central O atom. Feature *A* is reproduced by using solely the first Fe shell and has basically the same origin as peak *A* in α-Fe_2O_3 and Fe_3O_4, but with only a single broad component.

The intrashell multiple scattering within the first oxygen shell does produce the *B* peak as in the case of α-Fe_2O_3 and Fe_3O_4. Peak *C*, located 6.805 eV higher in energy than peak *B* arises approximately from single-scattering events between the absorber and the outer lying oxygen shell located at about 5.266 Å as expected. Peak *D* is due to single scattering from nearest neighbor oxygen shell. It is rather sharp due to the FeO rocksalt structure.

D. The prepeaks intensities

The intensity of the feature *A* relative to peak *B* increases in going from FeO to α-Fe_2O_3 [see Fig. 1(a)], and reflects the increased number of unoccupied 3*d* states available for

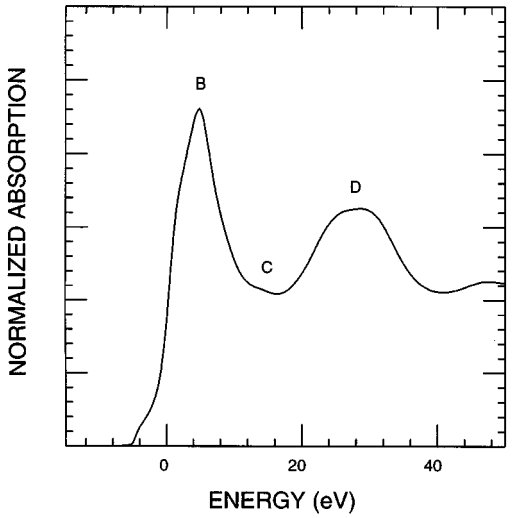

FIG. 8. MS calculation of O K-edge XANES in α-Fe_2O_3 by taking into account only 37 oxygen atom contributions (same cluster size used as the upper curve in Fig. 2 but without all Fe atoms).

mixing with the O $2p$ states and the decrease of the Fe-O bond length. This fact has already been observed by Colliex *et al.*[2] Likewise, Kurata *et al.*[8] and de Groot *et al.*[7] have observed a monotone decrease of the intensity of feature A over the TM series as a function of the number of accessible vacant d states.

As has been pointed out by de Groot *et al.*[7] several effects must be considered to account for the relative intensities of peaks A_1 and A_2. Starting from the high spin configuration of iron in α-Fe_2O_3 and FeO, one can first speculate that the A_1 and A_2 peak intensities are related to the number of $3d$ holes on iron, modulated by hybridization effects since, as mentioned above, the prepeak comes from the hybridization of the $2p$ oxygen orbitals with the $3d$ ones of iron. In α-Fe_2O_3, there are $3t_{2g}$ and $2e_g$ holes on iron. Without hybridization, a ratio of 3:2 for the peak intensities is therefore expected. As the e_g orbitals point towards the oxygen ligands, the O $2p$-e_g hybridization is stronger than the O $2p$-t_{2g} one, so that a ratio of about 1:1, as experimentally observed, does not seem to be unreasonable. However, in FeO, the ratio of t_{2g}/e_g holes is 2:2, and one could expect the prepeak to show two components, the intensity ratio of which is less than 2:2 (about 1:2, for instance), when taking into account hybridization. As this is not observed experimentally, we have to consider other effects. Indeed the effect of electronic interactions, especially the exchange term, must not be forgotten: as there is one more electron on iron in FeO than in α-Fe_2O_3, electronic interactions are very different in the two oxides, the more so as the d^5 iron ionic configuration in α-Fe_2O_3 is a special case. Indeed, as the d orbitals are half filled with five spin up electrons, the electronic interactions do not lead to a supplementary d splitting, so that the t_{2g}-e_g splitting keeps some meaning. This is not the case for d^6 ions, as in FeO, for which it has been shown that supplementary splittings appear due to electronic interactions, so that it has no meaning to speak about a simple t_{2g}-e_g splitting.[27] The splittings of the d orbitals is therefore complex and this could explain the broad shape of the prepeak A in FeO, this broadening being enhanced by solid state effects. Another effect that must be kept in mind is the nonstoichiometry effect: it is well known that FeO is very often iron defective. This fact has little consequence on the general shape of the O K XANES spectrum, since this latter is dominated by scattering between oxygen atoms (see Sec. V E), but might possibly influence the shape of the prepeak which is due to O $2p$- Fe $3d$ hybridization. Let us note however that, as the prepeak is not split in the MS calculation, this last hypothesis does not seem to be able to explain the occurrence of only one broad peak.

As already mentioned, the occurrence of three iron sites in Fe_3O_4 may lead to an intermediate case between Fe_2O_3 and FeO, due to the mixing of the contributions from each site.

E. Further considerations on features *B*, *C*, and *D*

In this section we want to substantiate in a more quantitative way the interpretation given above concerning the spectral features B, C, and D. We have indeed suggested that feature B is due to multiple scattering, up to infinite order, of the final state photoelectron in the cage of the first oxygen shell, so that it can be called ''a scattering resonance.'' On the contrary, features C and D appear to be ''diffraction'' maxima in the absorption coefficient due mainly to single-scattering events between the central absorbing atom and oxygens located on average at around 5 and 3 Å, respectively. That these features are due only to the oxygen cage in these oxides is demonstrated in Fig. 8, where they appear in a cluster calculation for α-Fe_2O_3 in which all Fe atoms have been eliminated.

As discussed more at length in Ref. 22, the difference between a scattering resonance and a diffraction maximum lies in the number and the coherence of the various scattering signals involved in the spectral feature. In a resonance very many (sometimes an infinite number of) ''diffractive'' signals, arising from individual MS paths, interfere coherently at a definite energy, called resonance energy, giving rise to a rather intense and sharp feature in the absorption coefficient. On the contrary in a diffractive maximum only signals from one or a few MS paths contribute with little or no coherence.

In the case of a scattering resonance it is known[28] that the energy position of the resonance E_r (measured from the origin of the photoelectron kinetic energy) and the linear dimension R of the confining shell are linked by the relation

$$E_r \cdot R^2 = \text{const.} \tag{1}$$

This equation relates therefore E_r and R in different materials, provided the nature of the scattering atoms involved in the resonance and their geometrical arrangement does not change substantially from one compound to the other.

This is indeed the case for our three oxides and Table III shows that for the scattering resonance B the energy position scales as the inverse square of the radius of the first oxygen shell R. Energies have been measured from the bottom of the conduction band, which coincides with the onset of the absorption in these compounds [around 530 eV from Fig. 1(a)] and with the average interstitial potential, as calculated by our program [-10 eV with respect to the vacuum level, as seen from Fig. 1(b)] (see also Ref. 8). Notice that the above relation can also be derived in an intuitive manner by imposing the condition that the phase $kR_{\text{tot}}+\Phi$ (where Φ indicates the sum of the scattering phase and the central atom phase shift) of the various MS paths interfering coherently at the resonance differ at most by a factor of 2π.[29] By this method

TABLE III. The ΔE (in eV) of peak B and the corresponding distances (in Å) of the oxygen first shell in α-Fe_2O_3, Fe_3O_4, and FeO.

Peak B	α-Fe_2O_3	Fe_3O_4	FeO
ΔE (eV) [a]	14.0	13.0	12.0
$\overline{R}$ (Å)	2.87	2.97	3.04
k (Å^{-1})	1.92	1.85	1.78
$\Delta E\overline{R^2}$ (eV Å^2)	115.3	114.6	111.0
$k\overline{R}$	5.5	5.5	5.4

[a]ΔE is measured from the onset of the absorption spectra.

one can even calculate ''*a priori*'' the value of the constant and compare with the experiments, provided that the nature of the coherent MS paths involved in the resonance is known. An analysis of resonance B in various oxides along these lines is being performed and will constitute the object of a future publication.

Concerning features C and D, it has been shown that they are mainly associated with EXAFS-like (single-scattering) signals of the form

$$A(k,R)\sin[2kR+\Phi(k,R)], \tag{2}$$

so that their maxima must lie at energy positions such that

$$2k_1R_1+\Phi_1(k_1,R_1)=2k_2R_2+\Phi_2(k_2,R_2)+2n\pi, \tag{3}$$

where 1 and 2 now refer to features C and D, respectively. Again the origin of the kinetic energies is at the bottom of the conduction band.

Table IV shows that this relation is satisfied with $n=1$ in all three oxides, since we have explicitly calculated that $\Phi_1(k_1,R_1)-\Phi_2(k_2,R_2)=0.14$ rad so that $\Delta(kR)=3.0$ rad of Table IV should be compared with $[\Phi_2(k_2,R_2)-\Phi_1(k_1,R_1)]/2+\pi=3.07$ rad.

We note that the appearance of the term $2n\pi$ in Eq. (3) is essential for the assignment of features C and D to the correct scattering shell. In fact the ratio of the respective shell distances from the central absorbing oxygen atom is $\sqrt{3}$, consistent with our MS calculations showing that peak C appears when the third oxygen shell is included in the model cluster.

This observation resolves also an apparent conflict found in Ref. 8, where on the basis of Eq. (1) applied to the corresponding features C and D in MnO, treated as scattering resonances with energy positions in the ratio of roughly 2 as in the present case, it was concluded that the respective shell distances were in the ratio $\sqrt{2}$, contrary to the finding by MS calculations.

As a last observation we point out that Eq. (3) can in principle be applied also to features B and D of the same compound, even though the first is a scattering resonance and the second a diffractive maximum. What makes the comparison possible is the fact that the single-scattering signal is one of the constituent signals of feature B and usually peaks at the same energy as the true resonance. From Tables III and IV we see that $\Delta(kR)$ ranges between 3.3 and 3.5 rad in the three oxides under consideration, with a calculated phase difference $\Delta\Phi/2$ of 0.1 rad. Given the approximations involved, the resulting value is reasonably close to π. This also indicates that in a certain sense feature D is the first harmonic of feature B whose signal has gone out of phase with all other MS signals present in B, being the only one surviving at a higher energy.

TABLE IV. The ΔE (in eV) of peaks C and D and the distances (in Å) of the corresponding oxygen shells in α-Fe_2O_3, Fe_3O_4, and FeO.

	α-Fe_2O_3		Fe_3O_4		FeO	
Peaks	C	D	C	D	C	D
ΔE (eV) [a]	21.5	37.5	20.15	33.5	18.8	32.0
k (Å^{-1})	2.38	3.14	2.31	2.97	2.23	2.89
$\overline{R}$ (Å)	5.04	2.87	5.14	2.97	5.27	3.04
$k\overline{R}$	12.0	9.0	11.82	8.82	11.8	8.8
$\Delta(k\overline{R})$	3.0		3.0		3.0	

[a]ΔE is measured from the onset of the absorption spectra.

VI. CONCLUSIONS

In conclusion, a detailed experimental and theoretical investigation of the O K edge XANES spectra has been performed on three different iron oxides, α-Fe_2O_3, Fe_3O_4, and FeO. We have obtained a reasonably good agreement between our data and one-electron full MS calculations for these edges. The variations of shape and intensity of the prepeaks have been analyzed in terms of electronic properties related to the occupation number of the $3d$ band, the site symmetry, and the bond length. We have also been able to identify the spectral features above the prepeaks, named B and D in Fig. 1(a), as arising from scattering of the photoelectron within the first oxygen coordination shell, the effect of the nearest neighbor Fe shell being negligible. While feature B is a true scattering resonance, due to multiple scattering up to an infinite order, feature D was identified instead as being a diffractive maximum, due mainly to a single-backscattering event. Feature C was also shown to be of diffractive origin and to be due to backscattering processes between the photoabsorber and the third oxygen shell. A relation has been established between the energy (and corresponding k vector) and the radius of the associated shell between these three features, both within the same spectrum for a particular oxide and between them. We have also shown how to resolve a contradiction found in Ref. 8 between the shell assignment for feature C by full MS calculations and that derived by an inappropriate application of the resonance relation in Eq. (1).

ACKNOWLEDGMENTS

We are grateful to A. Cooper, who kindly provided us with the α-Fe_2O_3 single crystal, previously grown by J.P. Remeika (AT&T Bell Laboratories). G. Dhalenne (Laboratoire de Chimie des Solides, Orsay, France) is gratefully acknowledged for supplying us with samples of Fe_3O_4 and FeO. We thank G. Tourillon, C. Laffon, and P. Parent (LURE, Orsay, France) for their help with the x-ray absorption experiments. This work was supported by a Human Capital and Mobility EC Grant (Z.Y.W.).

[1] A. Muan, Am. J. Sci. **256**, 171 (1957).
[2] C. Colliex, T. Manoubi, and C. Ortiz, Phys. Rev. B **44**, 11 402 (1991).
[3] J.H. Paterson and O.L. Krivanek, Ultramicroscopy **32**, 319 (1990).
[4] L.A. Grunes, Phys. Rev. B **27**, 2111 (1983).
[5] Y. Ma, P.D. Johnson, N. Wassdahl, J. Guo, P. Skitt, J. Nordgren, J.E. Rubensson, T. Böske, and W. Eberhardt, Phys. Rev. B **48**, 2109 (1993).
[6] S. Nakai, T. Mitsuishi, H. Sugarawa, H. Maezawa, T. Mattsukawa, S. Mitani, K. Yamasaki, and T. Fujikawa, Phys. Rev. B **36**, 9241 (1987).
[7] F.M.F. de Groot, M. Grioni, J.C. Fuggle, J. Ghijsen, G.A. Sawatzky, and H. Petersen, Phys. Rev. B **40**, 5715 (1989).
[8] H. Kurata, E. Lefèvre, C. Colliex, and R. Brydson, Phys. Rev. B **47**, 13 763 (1993).
[9] M. Pollak, M. Gautier, N. Thromat, S. Gota, W.C. Mackrodt, and V.R. Saunders, Nucl. Instrum. Methods Phys. Res. Sect. B **97**, 383 (1995).
[10] Th. Schedel-Niedrig, W. Weis, and R. Schlögl, Phys. Rev. B **52**, 17 449 (1995).
[11] J.P. Crocombette, M. Pollak, F. Jollet, N. Thromat, and M. Gautier-Soyer, Phys. Rev. B **52**, 3143 (1995).
[12] J. Stöhr, in *X-Ray Absorption: Principles, Applications, Techniques of EXAFS, SEXAFS,* edited by R. Prinz and D. Koningsberger (Wiley, New York, 1988), p. 443.
[13] P.J. Durham, in *X-ray Absorption: Principles, Applications, Techniques of EXAFS, SEXAFS, XANES* (Ref. 12).
[14] P.A. Lee and J.B. Pendry, Phys. Rev. B **11**, 2795 (1975).
[15] C.R. Natoli, D.K. Misemer, S. Doniach, and F.W. Kutzler, Phys. Rev. A **22**, 1104 (1980); C.R. Natoli, and M. Benfatto, J. Phys. (Paris) Colloq. **47**, C8-11 (1986); C.R. Natoli, M. Benfatto, and S. Doniach, Phys. Rev. B **34**, 4682 (1986); C.R. Natoli, M. Benfatto, C. Brouder, M.Z. Ruiz Lopez, and D.L. Foulis, *ibid.* **42**, 1944 (1990).
[16] Z.Y. Wu, M. Benfatto, and C.R. Natoli, Phys. Rev. B **45**, 531 (1992); Solid State Commun. **87**, 475 (1993).
[17] C.R. Natoli (unpublished).
[18] L. Mattheiss, Phys. Rev. A **134**, 970 (1964).
[19] E. Clementi and C. Roetti, At. Data Nucl. Data Tables **14**, 177 (1974).
[20] J. Desclaux, Comput. Phys. Commun. **9**, 31 (1975); J. Desclaux, J. Phys. B **4**, 631 (1971).
[21] P.A. Lee and G. Beni, Phys. Rev. B **15**, 2862 (1977).
[22] T.A. Tyson, K.O. Hodgson, C.R. Natoli, and M. Benfatto, Phys. Rev. B **46**, 5997 (1992), and references therein.
[23] J.C. Fuggle and J.E. Inglesfield, *Unoccupied Electronic States*, Topics in Applied Physics (Springer, Berlin, 1992), Appendix B, p. 347.
[24] D.R. Penn, Phys. Rev. B **35**, 482 (1987).
[25] J.G. Norman, *SCF-Xα Scattered Wave Calculation of the Electronic Structure of* $Pt(PH_3)_2O_2$ [Mol. Phys. **81**, 1191 (1974)].
[26] J. Ghijsen, L.H. Tjeng, J. Van Elp, H. Eskes, J. Wesrterink, G.A. Sawatzky, and M.T. Czyzyk, Phys. Rev. B **38**, 11 322 (1988).
[27] F.M.F. de Groot, Ph.D. thesis, University of Nijmegen, 1991.
[28] C.R. Natoli, in *EXAFS and Near Edge Structure*, edited by A. Bianconi, L. Incoccia, and S. Stipcich, Springer Series in Chemistry and Physics, Vol. 27 (Springer, Berlin, 1983), p. 43.
[29] J.J. Rehr, R.C. Albers, and S.I. Zabinsky, Phys. Rev. Lett. **69**, 3397 (1992).